Proceedings of 2004 JUSFA
2004 Japan - USA Symposium on Flexible Automation
Denver, Colorado, July 19-21, 2004

JL025

DISTURBANCE ESTIMATION ON A HEXAPOD-TYPE PARALLEL KINEMATIC MACHINE TOOL BY USING A DISTURBANCE OBSERVER

Toshihiro OKUDA, Soichi IBARAKI, Yoshiaki KAKINO
Department of Precision Engineering, Kyoto University
Yoshida-honmachi Sakyo-ku Kyoto, Japan 606-8501
Email: ibaraki@prec.kyoto-u.ac.jp

Masao NAKAGAWA, Tetsuya MATSUSHITA
Okuma Corp.
Oguchi-cho, Niwa-gun, Aichi, 80-0144 Japan

ABSTRACT

This paper presents a disturbance estimation methodology on a Hexapod-type parallel kinematic machine tool of the Stewart platform. The disturbance estimation by monitoring an armature current of servo motors has been commonly done on conventional serial mechanism feed drives. On a parallel mechanism feed drive, a disturbance observer must have a more complex structure with a precise model of the gravity effect on servo motor loads, which significantly varies depending on the position and the orientation of a spindle unit. The estimation performance of the proposed disturbance observer is validated through static load tests and cutting experiments. As an application example, the proposed disturbance estimation scheme is applied to the compensation of the tool deflection in end milling processes by tilting the spindle.

Key Words: parallel kinematic machine tools, Stewart platform, disturbance observer, servo motors, stiffness

1 Introduction

A commercial machine tool driven by a ”Hexapod”-type parallel kinematic feed drive was first introduced to the public in 1994. Although more than ten years have been passed since then, they are not widely accepted in today’s industry. One of critical issues with parallel kinematic machine tools is its lower stiffness against an external force, compared to conventional feed drives with a guideway that introduces higher friction. As parallel kinematic machine tools has begun to be accepted in the market lately, the improvement in their control performance in such an aspect is urgently needed.

In a parallel kinematic machine tool, a spindle unit is supported and driven only by struts without a guideway, which inherently makes it difficult to have higher stiffness, compared to conventional machine tools with a guideway. Although various design modification is possible to enhance the overall stiffness of a parallel kinematic drive, the stiffness issue still remains as a critical problem in most commercial parallel kinematic machine tools. For example, the installment of a ball screw of larger diameter naturally enhances the overall stiffness, although it costs more. Unlike the ”Hexapod”-type parallel kinematic drive, a parallel kinematic drive with movable base joints can have a guideway for each feed drive, and thus it typically exhibits higher overall stiffness. There are a considerable number of commercial machines adopting this structure [1]. Due to its more complicated structure, however, it is often more difficult to calibrate kinematic parameters on such a machine, and thus to achieve higher positioning accuracy. A comprehensive review on structures, issues, and applications of parallel kinematic machine tools can be found in [1].

This paper presents a disturbance estimation methodology using a disturbance observer on a Hexapod-type parallel kinematic machine tool of the Stewart platform. Most of research efforts found in the literature on the motion control of a parallel kinematic machine tool focuses on its static positioning performance. The identification of kinematic parameters is the most important issue in such an aspect[2]. On the other hand, there have been fewer works on the feedback control explicitly taking account of the dynamics of a parallel mechanism. If an external force acting on a spindle unit can be estimated accurately, we may be able to implement a control scheme to dynamically compensate it. Furthermore, on a parallel kinematic drive, it is well known that the gravity imposes a critical effect on its positioning accuracy[3]. The disturbance estimation plays an important role in the compensation of such an error. The autonomous monitoring and adaptive control of machining processes have been an active research issue in years from the viewpoint of the development of autonomous manu-

facturing systems[4]. The monitoring of cutting forces is one of key technologies in such a system for any types of machine tools. A disturbance observer will be of practical importance in these applications.

The remainder of this paper is organized as follows. The following section briefly reviews the configuration and the kinematics of a Hexapod-type parallel kinematic machine tool with the Stewart platform. The configuration of a disturbance observer for this parallel kinematic feed drive is presented in Section 3. Section 4 presents the experimental validation of the proposed estimation method. Section 5 presents the application of the proposed scheme to the compensation of tool deflection in two dimensional endmilling. Section 6 gives the conclusion of this paper.

2 Configuration and Kinematics of a Hexapod-type Parallel Kinematic Machine Tool

2.1 Configuration of a Hexapod-type Parallel Kinematic Machine Tool

This paper considers a Hexapod-type parallel kinematic machine tool of the Stewart platform[5] depicted in Figure 1. It has six telescoping struts, each of which is connected to a base plate by a 2-DOF joint. The other end of a strut is connected by a 3-DOF joint to a platform plate, where a spindle is installed.

Figure 2 shows a schematic view of COSMO CENTER PM-600 by Okuma Corp., a commercial Hexapod-type parallel kinematic machining center with the Stewart platform, which is used as an experimental machine throughout our study. Table 1 shows its major specifications. Each strut is driven by a built-in servo motor via a ball screw. The "length" of each strut is indirectly measured by a rotary encoder installed in a servo motor. In this paper, six joints on the platform plate are referred to as platform joints, while those on the base plate are referred to as base joints.

2.2 Inverse and Forward Kinematics of the Stewart Platform

In Figure 1. $\boldsymbol{T} = [X, Y, Z, A, B, C]$ represents the position and the orientation of the spindle tip (tool tip). When $\boldsymbol{T}$ is given, a problem to calculate the length of each strut, $\boldsymbol{L} = [L_1, \cdots, L_6]$, is called the inverse kinematic problem. Write it as:

$$\boldsymbol{L} = \mathcal{F}(\boldsymbol{T}) \tag{1}$$

where $\mathcal{F}$ represents the inverse kinematic function of the Stewart platform. Note that $\mathcal{F}$ is a function of the location of platform joints, $\boldsymbol{P}_j \in \mathbb{R}^3$ $(j = 1 \sim 6)$, and the location of base joints, $\boldsymbol{Q}_j \in \mathbb{R}^3$ $(j = 1 \sim 6)$. The inverse kinematic problem for the Stewart platform can be algebraically solved[2]. On the other hand, a problem to calculate $\boldsymbol{T}$ for the given $\boldsymbol{L}$ is referred to as the forward kinematic problem:

$$\boldsymbol{T} = \mathcal{F}^{-1}(\boldsymbol{L}) \tag{2}$$

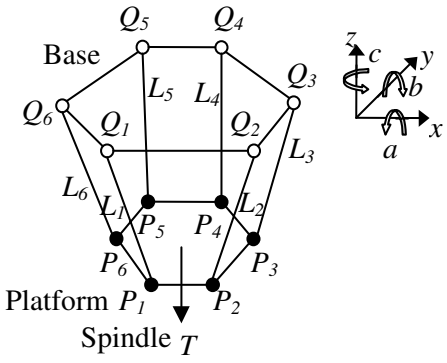

Figure 1. Stewart platform

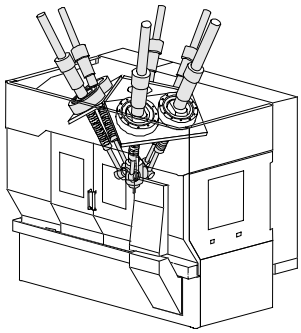

Figure 2. A Hexapod-type parallel kinematic machine tool, COSMO CENTER PM600.

Table 1. Major specifications of PM-600

Workspace, mm	ϕ600 (XY) $\times$400 (Z) ($420 \times 420 \times 400$)
Tilting angle, deg	± 25
Max. rapid traverse speed, m/min	100
Max. acceleration, m/s^2	14.7
Spindle speed, min^{-1}	12,000/30,000
Spindle power, kW	6

The forward kinematic problem of the Stewart platform cannot be algebraically solved. In our simulator, the Newton-Raphson method is employed to numerically solve it.

3 Disturbance Estimation using a Disturbance Observer

3.1 An Estimation Method in Parallel Mechanism

The disturbance estimation by monitoring armature current of servo motors has been commonly done on conventional serial mechanism feed drives[7]. As an example, we consider a single-axis feed drive which has a slideway driven by a servo motor via a ball screw. If the bandwidth of torque control loop for a servo motor can be assumed sufficiently wide, then we can simply assume that the motor torque is proportional to its armature current. That is, for the armature current (in A), the cutting force $\hat{d}$ (in N) can be estimated as follows:

$$\hat{d} = \frac{1}{R}\, K_t\, i - \hat{F} - \hat{f} \tag{3}$$

where $\hat{f}$ represents the estimated value of a friction force (N) acting on e.g. a slideway. $\hat{F}$ represents the estimated value of the inertial force (in N). K_t represents the motor's torque constant (Nm/A). $R(= \frac{P}{2\pi}$, P: all screw pitch(mm)) represents the coefficient to translate the rotary motion into the linear motion. In orthogonal-axis serial mechanism feed drives, the cutting force in the direction of each axis can be estimated by monitoring the armature current in each servo motor.

In parallel kinematic feed drives, unlike serial kinematic feed drives, 1) the cutting force acting on the spindle tip (or tool tip) must be estimated as the superposition of the force acting on each servo motor. 2) The gravity imposes a critical effect on Eq.(3), and its effect significantly varies depending on the position and the orientation of the spindle[6]. Therefore, it is necessary to estimate this effect precisely. 3) There is a variety of factors such as the friction on a ball screw and a joint that impose coupled effects over multiple axes. If these differences are regarded, the basic idea about the estimation of cutting forces shown above can be also applied to parallel kinematic feed drives. That is, using an armature current (in A) in the servo motor of the j-th strut, i_j ($j = 1 \sim 6$), the disturbance force in the direction of the j-th strut can be estimated as follows:

$$\hat{d}_j = \frac{1}{R} K_t \, i_j - \hat{F}_j - \hat{f}_j - \hat{g}_j \tag{4}$$

where $\hat{g}_j$, $\hat{F}_j$, $\hat{f}_j$ represent the gravity (in N), the inertial force (in N), and the friction force (in N) acting on the direction of j-th strut, respectively. The estimated cutting force acting on the spindle, $\hat{\boldsymbol{d}}$, is given as the superposition of the forces above. That is,

$$\hat{\boldsymbol{d}} = \sum_{j=1}^{6} \hat{d}_j \, \boldsymbol{l}_j \tag{5}$$

where $\boldsymbol{l}_j \in \mathbb{R}^3$ represents the unit vector in the direction of the j-th strut.

3.2 Configuration of a Disturbance Observer

As shown in Eq.(4) and (5), to estimate the cutting force $\hat{\boldsymbol{d}}$ on the parallel mechanism, it is necessary to estimate the gravity, $\hat{g}_j$, the friction force, $\hat{f}_j$, and the inertial force, $\hat{F}_j$ on all the struts for the given position and orientation of the tool tip.

3.2.1 A Gravity Model on Each Strut

At first, for the convenience of notation, define the following function, $\Gamma_{\boldsymbol{l},\boldsymbol{B}}(x) : \mathbb{R}^6 \rightarrow \mathbb{R}^6$ by:

$$\Gamma_{\boldsymbol{l},\boldsymbol{B}}(x) = \begin{bmatrix} \sum_{j=1}^{6} (x_j \boldsymbol{l}_j) \\ \sum_{j=1}^{6} (\boldsymbol{B}_j \times x_j \boldsymbol{l}_j) \end{bmatrix} \tag{6}$$

where $\boldsymbol{l}_j \in \mathbb{R}^3$ ($j = 1 \sim 6$) represents the unit vector in the direction of the j-th strut. $\boldsymbol{B}_j \in \mathbb{R}^3$ ($j = 1 \sim 6$) represents the location of the center of the j-th platform joint with respect to the center of gravity of the platform plate. Note that $\boldsymbol{l}_j$ and $\boldsymbol{B}_j$ are dependent on the tool position and orientation, $\boldsymbol{T}$. The symbol $\times$ denotes the outer product of two vectors. Notice that when x_j represents an axial force on the j-th strut, the first three components of the vector $\Gamma_{\boldsymbol{l},\boldsymbol{B}}(x)$ define the combined force vector of the axial forces. The last three components define the combined moment around the center of gravity of the platform plate imposed by the axial forces acting on platform joints.

The gravity imposed on the j-th platform joint in the direction of the j-th strut, $\hat{\boldsymbol{g}} = \{\hat{g}_j\}_{j=1\sim6}$, is given by solving the following equilibrium equation of force and moment around the center of gravity of the platform plate:

$$\Gamma_{\boldsymbol{l},\boldsymbol{B}} (\hat{\boldsymbol{g}} - \boldsymbol{g_s}) = \begin{bmatrix} -\boldsymbol{N_g} \\ -\boldsymbol{M_g} \end{bmatrix} \tag{7}$$

where $\boldsymbol{N_g} \in \mathbb{R}^3$ and $\boldsymbol{M_g} \in \mathbb{R}^3$ respectively represent an equivalent force and moment around the center of gravity of the platform plate given by the gravity acting on each strut. They are given as follows.

Figure 3 illustrates a gravity model on each strut. In the figure, m_P, m_B, m_J, m_S represent the mass (in kg) of the platform plate, the ball screw, the platform joint, and the servo motor, respectively. l_1 is the distance (in meter) between the rotation center of a base joint and the center of gravity of a servo motor, l_2 is the length of the platform joint unit on a strut, and l_3 is the length of the ball screw (distance between the rotation center of a base joint and a platform joint), and the L_j is the total length of the j-th strut. By using this model, $\boldsymbol{N_g}$ and $\boldsymbol{M_g}$ are given as follows:

$$\boldsymbol{N_g} = m_P \boldsymbol{g} + \sum_{j=1}^{6} \boldsymbol{N_{g,j}}, \quad \boldsymbol{M_g} = \sum_{j=1}^{6} \boldsymbol{M_{g,j}} \tag{8}$$

where $\boldsymbol{g} \in \mathbb{R}^3$ is a vector that represents the direction and the magnitude of the gravity. On each strut, the superposition of the gravity acting on a ball screw, a platform joint, and a servo motor can be represented as an equivalent moment around the rotation center of a base joint (see Figure 3). On the j-th strut, this moment imposes an equivalent force, $\boldsymbol{N_{g,j}}$ in Eq. (8), at the center of the j-th platform joint in the direction perpendicular to the strut. Similarly, $\boldsymbol{M_{g,j}} \in \mathbb{R}^3$ represents an equivalent moment around the center of gravity of the platform plate imposed by $\boldsymbol{N_{g,j}}$ on the j-th strut. That is,

$$\begin{aligned} \boldsymbol{N}_{g,j} &= \left\{ \frac{m_B \left(L_j - l_2 - \frac{l_3}{2}\right) + m_J L_j - m_S l_1}{L_j} \right\} \boldsymbol{g} \\ &\quad - \left[\left\{ \frac{m_B \left(L_j - l_2 - \frac{l_3}{2}\right) + m_J L_j - m_S l_1}{L_j} \right\} \boldsymbol{g} \cdot \boldsymbol{l}_j \right] \boldsymbol{l}_j \\ \boldsymbol{M}_{g,j} &= \boldsymbol{B}_j \times \left\{ \frac{m_B \left(L_j - l_2 - \frac{l_3}{2}\right) + m_J L_j - m_S l_1}{L_j} \right\} \boldsymbol{g} \\ &\quad - \boldsymbol{B}_j \times \left[\left\{ \frac{m_B \left(L_j - l_2 - \frac{l_3}{2}\right) + m_J L_j - m_S l_1}{L_j} \right\} \boldsymbol{g} \cdot \boldsymbol{l}_j \right] \boldsymbol{l}_j \end{aligned} \tag{9}$$

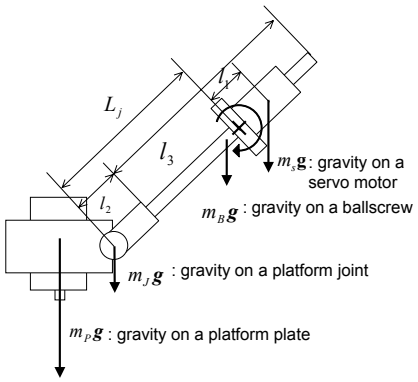

Figure 3. A gravity model on a strut and a platform.

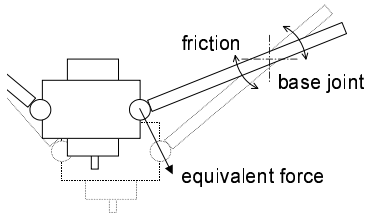

Figure 4. The friction on a base joint.

In Eq. (7), the j-th component of the vector $\boldsymbol{g_s} \in \mathbb{R}^6$ represents the axial component of the gravity acting on the j-th strut. It is given by:

$$\{\boldsymbol{g_s}\}_j = m_T\, \boldsymbol{g} \cdot \boldsymbol{l_j} \tag{10}$$

where m_T represents the total mass of one strut.

3.2.2 A Friction Model on Each Strut On each strut, we consider: 1) a linear friction on a ball screw, and 2) an angular friction in a base joint. The total friction force in the direction of j-th strut, $\hat{\boldsymbol{f}} = \{\hat{f}_j\}_{1\sim6}$, is given by solving the following equation:

$$\Gamma_{\boldsymbol{l},\boldsymbol{B}}(\hat{\boldsymbol{f}} - \boldsymbol{f_b}) = \begin{bmatrix} -\boldsymbol{N_c} \\ -\boldsymbol{M_c} \end{bmatrix} \tag{11}$$

where $\boldsymbol{f_b} \in \mathbb{R}^6$ represents a linear friction (in N) between a ball screw and a nut, and is given by the following simple model:

$$\{\boldsymbol{f_b}\}_j = -f_{0j}\ \mathrm{sign}\left(\dot{L}_j\right) \tag{12}$$

where f_{0j} is constant. $\dot{L}_j$ represents the axial velocity of the j-th strut. f_{0j} may depend on the velocity or the direction of the strut. On our experimental machine, however, such an effect was sufficiently small and thus is neglected for the simplicity of the model.

In Eq. (11), $\boldsymbol{N_c}$, $\boldsymbol{M_c} \in \mathbb{R}^3$ respectively represent an equivalent force and moment around the center of gravity of the platform plate given by an angular friction in each base joint. As illustrated in Figure 4, an angular friction in a base joint is modeled as an equivalent force acting on the platform joint in the direction perpendicular to the strut. $\boldsymbol{N_c}$ represents the superposition of such forces, and $\boldsymbol{M_c}$ represents the superposition of moments around the center of gravity of the platform plate imposed by such forces. That is,

$$\begin{aligned} \boldsymbol{N}_c &= -\sum_{j=1}^{6} \frac{t_{0j}}{L_j} \frac{d\left(L_j \boldsymbol{l}_j\right)/dt}{\left|d\left(L_j \boldsymbol{l}_j\right)/dt\right|} \\ \boldsymbol{M}_c &= -\sum_{j=1}^{6} \boldsymbol{B}_j \times \frac{t_{0j}}{L_j} \frac{d\left(L_j \boldsymbol{l}_j\right)/dt}{\left|d\left(L_j \boldsymbol{l}_j\right)/dt\right|} \end{aligned} \tag{13}$$

where t_{0j} is the friction torque acting on the base joint of j-th strut (Nm).

3.2.3 Inertial Force The inertial force in the direction of j-th strut, $\hat{\boldsymbol{F}} = \{\hat{F}_j\}_{1\sim6}$, is given by solving the following equation:

$$\Gamma_{\boldsymbol{l},\boldsymbol{B}}\left(\hat{\boldsymbol{F}}\right) = \begin{bmatrix} -\boldsymbol{N_F} \\ 0 \end{bmatrix} \tag{14}$$

where $\boldsymbol{N_F} \in \mathbb{R}^3$ represents a inertial force (in N) imposed on the spindle tip (tool tip). If the acceleration of the spindle tip is low, the inertial force becomes sufficiently small compared to the gravity and the friction, and thus can be neglected.

3.2.4 Estimation of Cutting Forces and Identification of the Estimation Model To summarize the discussion above, when the position and the orientation of the tool tip, $\boldsymbol{T}$, are given, the axial force on each strut can be estimated as follows: 1) for the given $\boldsymbol{T}$, compute the orientation of struts, $\boldsymbol{l}$, and the position of platform joints with respect to the center of gravity of the platform plate, $\boldsymbol{B}$, by solving the inverse kinematic problem. 2) Calculate $\hat{\boldsymbol{g}}$, $\hat{\boldsymbol{f}}$ and $\hat{\boldsymbol{F}}$ by algebraically solving Eqs. (7) , (11) and (14), respectively. 3) For the measured motor current in the j-th servo motor $i_j (j = 1 \sim 6)$, the disturbance force, $\hat{\boldsymbol{d}}$, is given by Eqs. (4) and (5).

Some of the parameters included in the estimation model must be experimentally identified as follows. The parameters, m_S in Eq. (9), m_T in Eq. (10), f_{0j} in Eq. (12), and t_{0j} in Eq. (13), are to be identified by performing simple identification tests, where the armature current in servo motors are measured in circular operations under a couple of different conditions. Then, the parameters are identified such that an error between measured and simulated profiles of the motor load on each strut is minimized see Section 4.1. Other parameters are set to the design values.

4 Experimental Validations

4.1 Estimation of the Armature Current in Servo Motors in a Circular Operation

To estimate cutting forces accurately using the proposed disturbance observer, it must be capable of simulating servo motor loads in a sufficient accuracy when it is subject to no cutting load. The validity of the proposed dynamic model is experimentally verified on the Hexapod-type parallel kinematic machine tool shown in Section 2.1 by comparing measured and simulated armature current in servo motors.

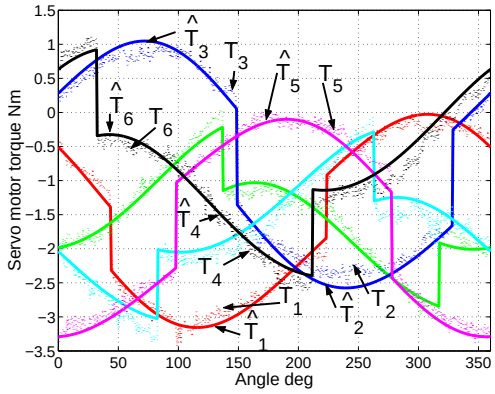

(a) Center location (X,Y,Z)=(0,100,-1008) (mm), tilting angle (A,B)=(0,0) (deg).

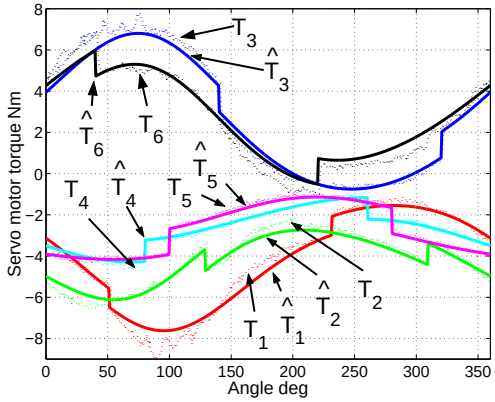

(b) Center location (X,Y,Z)=(0,100,-1008) (mm), tilting angle (A,B)=(-23,0) (deg).

Figure 5. Comparison of measured (T_i) and simulated ($\hat{T}_i$) servo motor torque profiles on each strut ($i = 1 \sim 6$) in a circular operation.

Figure 5(a)(b) show servo motor torque profiles ($T_1 \sim T_6$)($= K_t \cdot i_j$ in Eq.(4)) and their estimates ($\hat{T}_1 \sim \hat{T}_1$)($= R(\hat{F}_j + \hat{f}_j + \hat{g}_j)$ in the same equation) in circular operations. These tests were conducted with the same center location and radius, but with different spindle's tilting angles. In both tests, the feedrate was 1,000 mm/min, the reference trajectory radius was 144 mm, and the rotation direction was CCW (counter clockwise). It can be observed that unlike serial kinematic feed drives, servo motor loads in a parallel kinematic feed drive drastically vary as the position and orientation of the spindle change. However, there are good agreements between the measured and estimated motor load profiles, which validates the estimation performance of the proposed disturbance observer in an operation subject to no cutting force.

4.2 Estimation of a Static External Force

As the machine stays stational, a static force is imposed on a platform plate. The force is measured by using a load gauge, and is compared with its estimate by using the disturbance observer based on measured servo motor currents. The test procedure is as follows: an external force loaded on a platform plate is increased from 0 N to 3.5N by 0.5N, and then is decreased to 0N by 0.5N. The same test is repeated in the X and Y directions.

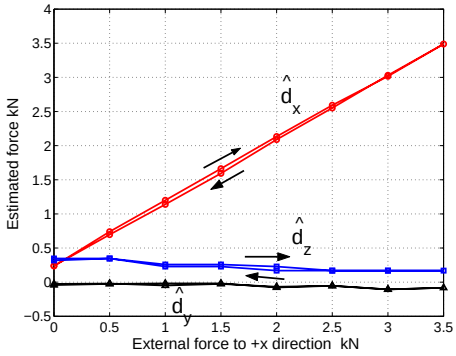

(a) For an external force imposed to the +X direction.

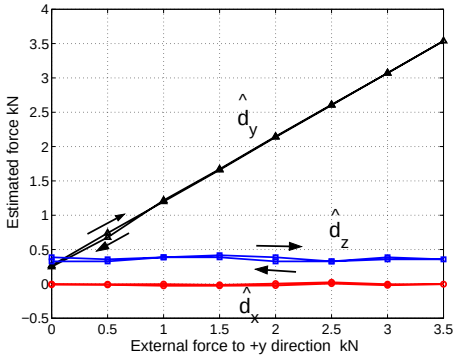

(b) For an external forces imposed to the +Y direction.

Figure 6. The estimate of the static external force (its X-, Y-, and Z-components are respectively compared with the actual force).

Figure 6(a)(b) shows the comparison of estimated external forces, $\hat{d}_x$, $\hat{d}_y$, $\hat{d}_z$, (vertical axis) and actual forces (horizontal axis) when the static forces are loaded on X and Y directions, respectively. Although the estimation error in Z direction, which must be ideally zero, is relatively large mainly due to modeling errors in the static friction in the proposed estimation model, this error is of no importance in practice. The estimation error in the direction where the external force is loaded is about 240 N at maximum and the error becomes smaller as the force becomes larger.

4.3 Estimation of the Cutting Forces

Cutting experiments are conducted in the condition shown in Table 2. Estimated forces by the disturbance observer are compared with the actual forces measured by a 3 component dynamometer in the straight end milling test to X and Y directions with various radial depth of cut shown in the table.

As examples, figure 7 shows a comparison of measured

Table 2. Cutting conditions

Workpiece material	Aluminum alloy, A5052
Tool	A sintered carbide square endmill (2 flutes, ϕ12mm)
Spindle speed	12,000 min^{-1}
Feedrate	6,000 mm/min
Milling method	Down cut
Axial depth of cut	18.0 mm
Radial depth of cut	1.0, 2.0, 2.5, 3.5, 4.0mm
Tool extension	130 mm (from spindle unit)

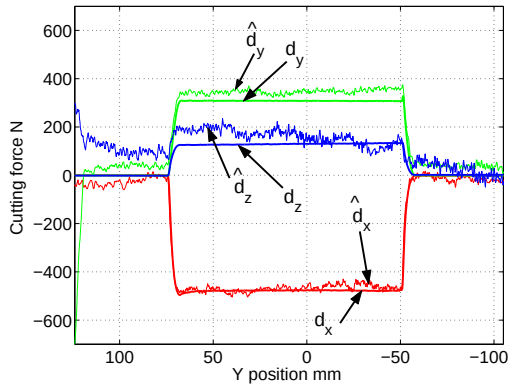

(a) Straight end milling toward -Y direction.

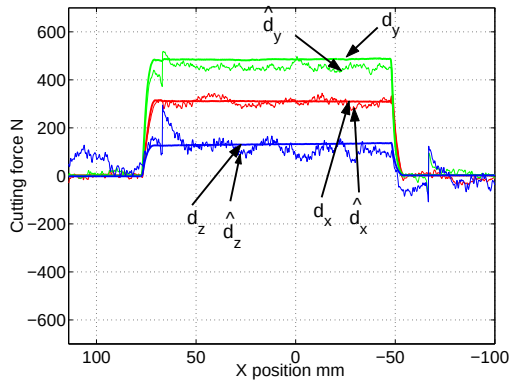

(b) Straight end milling toward -X direction.

Figure 7. Measured (d_x, d_y, d_z) and estimated ($\hat{d}_x$, $\hat{d}_y$, $\hat{d}_z$) cutting force profiles in straight end milling tests (radial depth of cut: 4.0mm).

and estimated cutting force components with the radial depth of cut of 4.0mm.

5 Application Example

5.1 Compensation of Tool Deflection

The tool is deformed by the cutting force in machining, which results in the inclination of the machined surface. As a "Hexapod"-type parallel kinematic machine tool is capable of 5-axis motion, by regulating the tilting angles of a spindle unit, we can potentially cancel the inclination of the machined

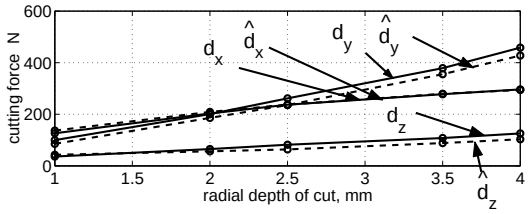

(a) Straight end milling toward -Y direction.

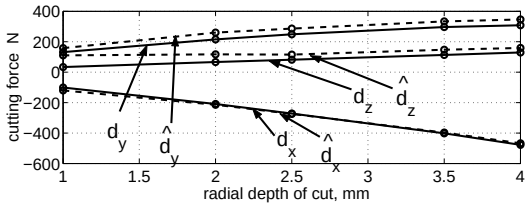

(b) Straight end milling toward -X direction.

Figure 8. Comparison of the mean value of measured (solid lines) and estimated (dashed lines) cutting forces in X, Y, and Z directions in straight end milling tests with various radial depth of cut.

surface for higher-accuracy machining. In this chapter, a basic experiment are conducted for validation of the estimation and the compensation method of the tool deflection using the proposed disturbance observer.

5.2 Estimation Method of the Tool Deflection

To obtain the relationship between the normal cutting force and the deflection of the tool, straight cutting tests toward the -Y direction were conducted in the condition shown in Table 2 and the inclination of the machined surface is measured by using a electric micrometer. Figure 9 shows measured surface profiles in +Z direction for the radius depth of cut of 0.1, 0.3, 0.5, 1.0, and 2.0 mm. The relationship between the normal cutting force and an inclination of the machined surface is summarized in Figure 10. In this figure, the inclination is defined as the angle between the line that connects the points at maximum and minimum of the deflection and the vertical line. In Figure 10, the relationship can be approximated by a quadratic function, which implies that the overall deflection can be modeled as a cantilever beam in a sufficient accuracy. In the following tests, this equation is used for the estimation of the tool inclination. To summarize, the estimation procedure of the tool deflection is as follows: The inclination of the machined surface, $\hat{\theta}$, and the deviation of the machined surface to the normal direction, $\hat{\delta}$, is given by the following equations.

$$\hat{\theta} = f(\hat{\boldsymbol{d}}_n) \tag{15}$$

$$\hat{\delta} = R_a \tan\hat{\theta} \tag{16}$$

where $\hat{\boldsymbol{d}}_n$ represents the normal component of the estimated cutting force, $\hat{\boldsymbol{d}}$. R_a represents the axial depth of cut. The function f represents the approximate curve in Figure 10. For the given command position (and orientation), estimate the error caused by the cutting force, $\boldsymbol{\Delta\hat{T}} = \left[\,\hat{\delta}\ 0\ 0\ 0\ \hat{\theta}\ 0\,\right]$, by using

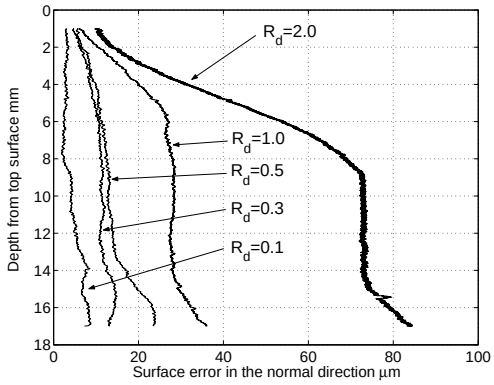

Figure 9. Surface profiles in the direction normal to the vertical surface with various radial depth of cut, R_d=0.1, 0.3, 0.5, 1.0, 2.0mm.

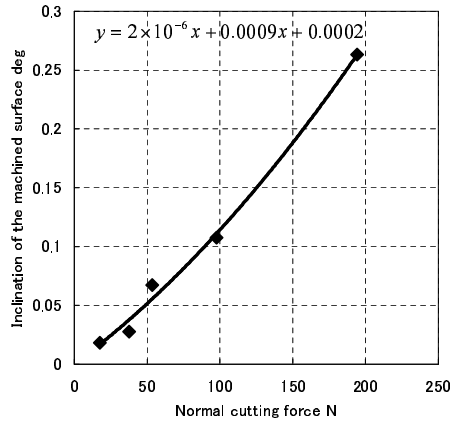

Figure 10. The relationship between the normal cutting force (in the X direction) and the inclination (around the Y axis) of the machined surface measured in the machining tests.

Eqs.(15)(16) (its direction depends on the feed direction. This example assumes the cutting toward -Y direction). The command position must be shifted to $\hat{\boldsymbol{T}}_{\boldsymbol{comp}} := \hat{\boldsymbol{T}} - \boldsymbol{\Delta}\hat{\boldsymbol{T}}$.

5.3 Experimental Results

Straight end milling test in -Y direction is conducted by using the workpiece that has a stairway-shaped surface as shown in Figure 11, such that the radial depth of cut varies from 0.3, 0.6, to 0.9 mm as the tool moves to -Y direction. Table 3 shows the mean value of cutting forces estimated by the measured servo motor torque and the inclination and deviation of the machined surface calculated by the normal cutting forces. The compensation of the tool deflection is not done. The mean value of actual forces measured by a dynamometer is also shown in the table.

Then cutting test under the compensation of the tool deflection is conducted with the compensation command calculated based on estimated cutting forces shown in Table 3. The machined surface is then measured by a electric micrometer in

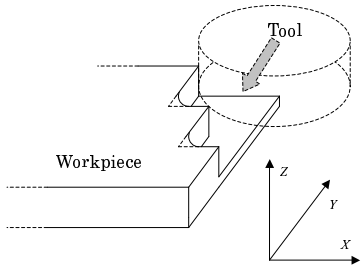

Figure 11. A schematic view of the machining test.

Table 3. Comparison of measured and estimated cutting forces and the compensation in the command trajectory with various radial depth of cut.

Radial depth of cut mm	Mean value of normal cutting force N		Compensation command	
	Measured	Estimated	X mm	B deg
0.3	37	38	-0.012	+0.038
0.6	63	58	-0.019	+0.060
0.9	91	76	-0.026	+0.083

+Z and -Y directions. Figures 12 and 13 show the surface error profiles without (a) and with (b) the compensation measured along the +Z and -Y direction, respectively. In Figure $13^{(b)}$, there are spike-shaped errors at distances 40mm and 80mm. They are caused by a brief stop of the spindle motion in order to change its tilting angle. In this experiment, this error is of no importance. By applying the compensation, the inclination of machined surface was reduced to near zero and the deviation of the surface error became less than 1/3.

6 Conclusion

This paper presented a disturbance estimation methodology on a Hexapod-type parallel kinematic machine tool of the Stewart platform using a disturbance observer. The following conclusion are drawn.

1. While a methodology to estimate a disturbance imposed on a feed drive from an armature current in servo motors has been done widely on a conventional orthogonal type serial kinematic feed drive, a disturbance observer for a parallel kinematic feed drive becomes more complex. Since a parallel kinematic feed drive has no linear guideway that is subject to higher friction, however, it is often easier to estimate cutting forces from servo motor currents than on a serial kinematic machine with guideways.
2. The estimation performance of the proposed disturbance observer was experimentally validated by static tests and straight cutting tests. A low-frequency component of the cutting force was estimated in a sufficient accuracy for all the directions. Although the estimation error in the Z direction was relatively large because of modeling errors,

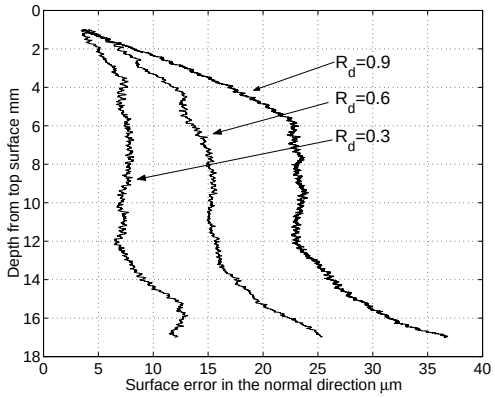

(a) Without the compensation.

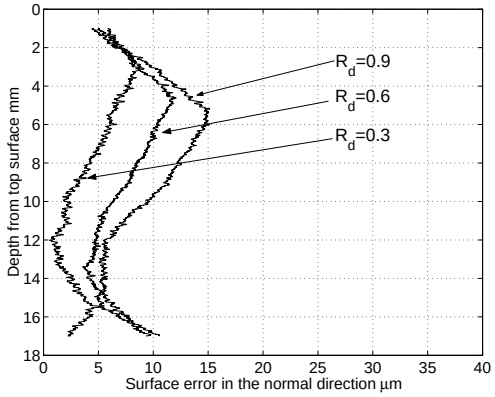

(b) With the compensation.

Figure 12. Comparison of surface error profiles with and without the compensation measured along the +Z direction (normal to the feed direction).

this error is of no importance in practice.

3. A compensation method of the tool deflection by the estimated cutting forces is presented. The tool deflection is estimated, and then the compensation command is calculated by subtracting these estimates from the reference trajectory. By applying the compensation, the inclination of machined surface was reduced to near zero and the deviation of the surface error became less than 1/3.

In our future research, we will consider the application of the proposed disturbance observer to the improvement of overall motion accuracy of a parallel kinematic feed drive, such as the compensation of gravity-induced errors.

ACKNOWLEDGMENT

This work was in part supported by the JSPS Grants-in-Aid for Scientific Research (#15560094).

REFERENCES

[1] Weck, M. and Staimer, D., Parallel Kinematic Machine Tools – Current State and Future Potentials, *Annals of the CIRP*, 51-2 (2002), 671–683.

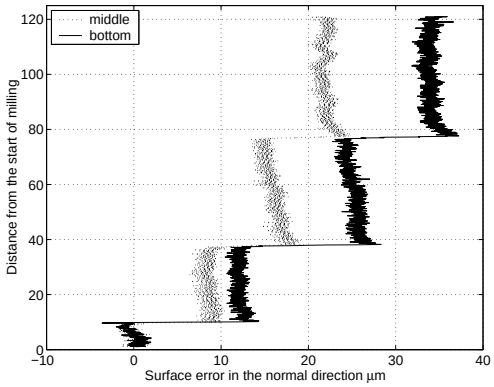

(a) Without compensation.

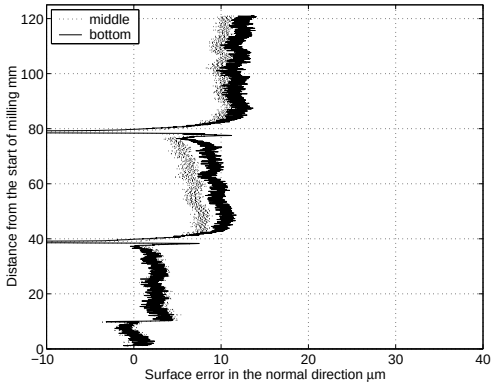

(b) With compensation.

Figure 13. Comparison of surface error in the normal direction with and without compensation measuring -Y direction.

[2] Nakagawa, M., Matsushita, T., Nashiki, M., Kakino, Y., Ihara, Y., A Study on the Improvement of Mo-tion Accuracy of Hexapod type Parallel Mechanism Machine Tool (1st Report), *J. of Jpn Soc. Prec. Eng.*, (in Japanese), Vol.67, No.8 (2001), pp.1333–1337.

[3] Ota, H., Shibukawa, T., Tooyama, T., Uchiyama, M., Study of Kinematic Calibration Method for Parallel Mechanism (3rd Report) –Gravity Compensation and Kinematic Calibration Considering Gravity, *J. of Jpn Soc. Prec. Eng.*, (in Japanese), Vol.66, No.10 (2000), pp.1568-1572.

[4] Matsubara, A., Current Status and Trends of Monitoring and Control Technology in Machining Processes, *Journal of the society of instrument and control engineers*, 41, 11 (2002)781–786.

[5] Stewart, D., A platform with six degree of freedom, *Proceedings of the Institution of Mechanical Engineering*, 180-1, 15 (1965), 371

[6] Nakagawa, M., Matsushita, T., Watanabe, S., Kakino, Y., Ihara, Y., The Improvement of Motion Accuracy of Hexapod Type Machine Tools and Its Machining Performance, *Proc. of 2002 Japan-USA Symp. on Flexible Automation*, vol. 2, (2002), pp. 979–982.

[7] Altintas, Y., Prediction of Cutting Forces and Tool Breakage in Milling from Feed Drive Current Measurements, *ASME Journal of Engineering for Industry*, 114 (1992), 386–392.